Fair-weather friends: Unequal partnerships between *Parastagonospora nodorum* and *Pyrenophora tritici-repentis* define disease dynamics in wheat

Running title: Unequal partners in wheat co-infection

Leon Lenzo [1], Evan John [2], Jason Bradley [3], Geoff Thomas [3], Dion Bennett [4,5] and Kar-Chun Tan [1*]

[1]Centre for Crop and Disease Management, School of Molecular and Life Sciences, Curtin University, Perth, Western Australia, 6102, Australia

[2]Department of Plant Pathology, Institute of Crop Science and Resource Conservation (INRES), University of Bonn, Nussallee 9, Bonn, 53115 Germany

[3]Department of Primary Industries and Regional Development, 6151, Perth, Western Australia, Australia

[4]Australian Grain Technologies, Northam, Western Australia, 6401, Australia

[5]School of Molecular and Life Sciences, Curtin University, Perth, Western Australia, 6102, Australia

*Corresponding author; Kar-Chun.Tan@curtin.edu.au

Keywords: *Parastagonospora nodorum*, *Pyrenophora tritici-repentis*, necrotrophic, fungal, pathogens, co-infection, septoria nodorum blotch, wheat, tan spot, yellow leaf spot, priority effects, digital PCR

Abstract

Parastagonospora nodorum and *Pyrenophora tritici-repentis* are the causal agents of septoria nodorum blotch and tan spot of wheat, respectively. Though these fungal phytopathogens have been found to frequently cohabitate the same leaf, their interaction dynamics in the manifestation of disease remain poorly understood due to limitations in species-specific detection methods. We developed a digital PCR based model targeting conserved regions of the α-tubulin gene, enabling biomass quantification of both pathogens during infection. Field surveys revealed up to two in three symptomatic infections involved both pathogens, with co-infected plants showing significantly higher individual pathogen biomass than single-species infections. Host plants in the field with moderate resistance to both pathogens were found to be significantly more necrotic under co-infection, with individual pathogen biomass up to twice that observed value for single infections. However, like fair-weather friends the partnership between these two pathogens seems to be conditional. When *P. tritici-repentis* established first, secondary *P. nodorum* colonisation led to a breakdown of host resistance. Conversely, when *P. nodorum* established on the host first, it suppressed *P. tritici-repentis* colonisation regardless of host resistance. To our knowledge this is the first description of asymmetric priority effects overcoming host resistance in a plant pathosystem. Resistance breeding strategies evaluating single pathogen challenges may inadvertently select for cultivars vulnerable to sequential co-infection, necessitating integrated disease complex approaches for durable resistance development.

Introduction

The order in which microorganisms colonise habitats fundamentally shapes community assembly and species interactions, a phenomenon known as priority effects [1]. In the colonisation of plant tissues, early arriving species modify environmental conditions and resource availability, altering biotic conditions to determine the trajectory of community development [2]. Agricultural phyllospheres represent a synthetic, simplified ecological context, where vast expanses of genetically homogeneous hosts grown at high density create conditions that accelerate pathogen evolution and promote rapid population growth [3]. Previous work

46 has demonstrated priority effects in plant-associated microbial communities, with pathogen arrival order
47 determines infection outcomes and host responses, yet their operation in agricultural pathosystems
48 remains poorly understood despite their potential to fundamentally alter disease outcomes [4,5]. Recent
49 surveys using molecular analysis across European wheat fields revealed that over two thirds of
50 symptomatic leaf samples harboured at least two pathogenic fungal species [6]. Environmental monitoring
51 studies using spore trapping showed propagules from fungal pathogens circulate simultaneously during
52 growing seasons, creating opportunities for co-infection [7]. While priority effects have been extensively
53 documented in bacterial pathosystems, with pathogens employing diverse strategies including
54 competition, cooperation, and temporal separation to succeed in polymicrobial environments, their
55 operation in fungal plant pathosystems remains poorly understood despite their potential to fundamentally
56 alter disease outcomes [8].Polymicrobial infections in plant systems may result in resource competition, host
57 immune modulation or direct pathogen-pathogen interactions that chemically or mechanically modulate
58 the colonization, reproduction, and transmission success of coinfecting species [9]. These interactions can
59 be either facilitative, where one pathogen creates conditions that enhance proliferation of another [10,11], or
60 inhibitory, where pathogens actively suppress competitors through antimicrobial compounds or resource
61 monopolization [12,13].
62
63 *Parastagonospora nodorum* and *Pyrenophora tritici-repentis*, the causal agents of septoria nodorum blotch
64 (SNB) and tan spot (TS) of wheat, represent an ideal system for investigating priority effects in necrotrophic
65 plant pathosystems [14,15], with previous work documenting near ubiquitous co-occurrence across wheat
66 growing regions [16]. Empirical studies of interactions between species have been limited however, largely due
67 to the morphological similarity of their constituent diseases and lack of robust quantitative methods. Both
68 pathogens are members of the order Pleosporales, which also includes pathogens such as *Leptosphaeria*
69 and *Alternaria* spp., and share similar infection strategies [17]. They each employ necrotrophic effectors that
70 interact with dominant host susceptibility genes to trigger an uncontrolled hypersensitive response,
71 resulting in necrotic lesions that support pathogen proliferation [18]. Notably, both species share the

72 necrotrophic effector ToxA, with evidence suggesting a horizontal gene transfer event, indicating stable
73 physical proximity between the two species [19]. Breeding efforts have made significant progress in improving
74 wheat resistance to both diseases through the elimination of dominant susceptibility genes such as *TaTsn1*,
75 which interacts with ToxA [20], and through the stacking of resistance alleles for both SNB and TS [21,22]. Despite
76 these advances, both diseases continue to persist in wheat-growing regions worldwide and remain priority
77 targets for resistance breeding [23], suggesting that current single-pathogen evaluation approaches may not
78 capture the complexity of field disease dynamics.
79
80 Previous efforts to study co-infection dynamics between these pathogens have faced significant
81 methodological constraints. Due to the morphological similarity of lesions produced by both pathogens,
82 and with coalescence obscuring distinct characteristics, visual assessment of disease symptoms requires
83 microscopic analysis even by trained pathologists [24,25]. Neural-network based disease identification
84 algorithms, which have achieved superior classification accuracy for other wheat diseases, have not yet
85 addressed the challenging differentiation between morphologically similar leaf spot diseases such as SNB
86 and TS [26]. The development of Real-Time Polymerase Chain Reaction (RT-PCR) assays to quantify both
87 pathogens in host tissue as well as the closely related hemi-biotroph *Zymoseptoria tritici* has provided
88 pioneering insight into the dynamics of foliar wheat pathogens during co infection [6,27,28]. However, these
89 studies rely on DNA as a direct analogue for pathogen biomass well as the utilization of targets with unstable
90 copy number in the genome including ribosomal and transposon associated sequences. For example, a
91 multicopy target for *P. tritici-repentis* [29] which was found to be variable across strains and regions (Figure S1)
92 [28]. Although this increases its sensitivity, it renders the assay unsuitable for field application where
93 uncharacterised strains may be present. Additionally, RT-PCR suffers from a lack of reproducibility at low
94 pathogens titre, especially in complex environmental samples where PCR inhibitors are known to be
95 present [30]. Digital PCR (dPCR) addresses limitations of RT-PCR by providing absolute quantification of target
96 nucleic acids without standard curves, offering greater precision and reproducibility while being more
97 tolerant of inhibitors and capable of reliably detecting low abundance targets[31].

98

99 Despite significant advances in breeding for resistance against SNB and TS, both *P. nodorum* and *P. tritici-*
100 *repentis* continue to persist in wheat-growing regions globally [6,16,23]. They are most commonly found under
101 co-infection conditions, suggesting that interactions between the two organisms may facilitate their
102 sustained proliferation. Consequently, SNB-TS wheat pathosystem has been a focal point and model of
103 research into polymicrobial infection of plants in recent years, where a range of RT-PCR-based targets have
104 been developed for pathogen monitoring and demonstrated a high field co-infection incidence [6,16,28]. It is not
105 known how wheat varieties that differ in resistance to TS and SNB dictate the outcome of single versus SNB-
106 TS co-infection, and so we sought to clarify whether *P. nodorum* and *P. tritici-repentis* form cooperative or
107 competitive associations during co-infection in wheat. We hypothesise that pathogen proliferation will be
108 determined by: (1) genetic resistance present in the host wheat leaves, (2) co-infecting pathogen presence
109 or absence and (3) pathogen arrival order. Here, we develop a duplex digital PCR assay alongside automated
110 image analysis enabling simultaneous absolute quantification of both pathogens from infected tissue and
111 apply these tools to investigate polymicrobial disease dynamics in a necrotrophic plant pathosystem.

112

113 **Materials and Methods**

114 ***Fungal Manipulations***

115 Reference isolates for *P. nodorum* SN15 [32] and *P. tritici-repentis* M4 [33] were used for all *in vitro* and defined
116 *in planta* inoculation in this study. All isolates were maintained on 90 mm V8 PDA plates [34], at ambient
117 temperature under a 12h light/dark photoperiod. To generate mycelial tissue, isolates were grown in Fries 3
118 broth [35]before lyophilisation . To generate inoculum, *P. nodorum* conidiospores were harvested directly from
119 V8PDA plates and resuspended in 0.02% w/v Tween . Inoculum for *P. tritici-repentis* isolates was generated
120 as previously described [36].

121

122 ***Visual Disease Analysis***

123 Harvested leaves were photographed *in situ* using a Google Pixel 6 Pro (USA). Individual leaf images were
124 manually extracted and catalogued using ImageJ [37]. Differential hue value masks were then generated to
125 distinguish between healthy, chlorotic and necrotic tissue, with cutoffs at 90, 43 and 30 respectively utilizing
126 the opencv library for Python. For full HSV values, refer to Table S1. The Python tools "LeafScan" for image
127 processing and analysis were developed and are available at https://github.com/LeonLenzo/leaf-scan.
128 Normalised pixel values to total leaf areas were used for downstream analyses.
129
130 ***Nucleic Acid Purification***
131 All fungal and plant tissues were snap frozen in liquid nitrogen and homogenized using a Tissue Lyser II
132 (Retsch, Duesseldorf, Germany), and DNA was purified using the Biosprint DNA Plant Kit in a Biosprint15
133 (both, Qiagen, Hilden, Germany) DNA concentrations were determined by fluorometric analysis using a
134 Qubit Flex system employing the dsBRDNA Working Solution (Thermofisher, Massachusetts, USA).
135
136 ***Digital PCR Assay***
137 Primers aT_F and aT_R were designed to simultaneously amplify a 187-bp region in *P. nodorum* and a 185-
138 bp region in *P. tritici-repentis*. These sequences were then used to query 179 *P. nodorum* [38,39] and 67 *P. tritici-*
139 *repentis* [14,40] genome assemblies to ensure within-species conservation and single copy status. Internal from
140 the primer-binding-site sequences, species-specific fluorescent probes Pn_FAM and Ptr_HEX were
141 designed to differentially amplify the target organisms (Table 1). Purified gDNA from *P. nodorum* SN15 and
142 *P. tritici-repentis* M4 were used to optimize the assay. dPCR reactions were carried out in 22-µl volumes,
143 where each well contained 11µl ddPCR Supermix for Probes (No dUTP) (Bio-Rad, California, USA), 5µl DNA
144 template, and 0.25µM of primer/probe mix at equimolar concentration. A QX200 Automatic Droplet
145 Generator (Bio-Rad, California, USA) was used to fractionate samples according to manufacturer's
146 instructions, before undergoing thermal cycling at 95°C for 10 min, then 40 cycles of 94°C for 30 s, 60°C for
147 60 s, then a final denaturation of 95°C for 10 min. The QX200 Droplet Reader (Bio-Rad, California, USA) was
148 used to quantify positive droplets, with data analysis performed using QuantaSoft Analysis Pro v1.0.596

149 (Bio-Rad, California) to determine absolute copy numbers following Poisson distribution correction. For
150 downstream analysis, copy per microlitre outputs were only counted for values >1, and all input DNA values
151 were normalised to 1ng/µl. In silico off-target analysis was performed by querying all primer and probe
152 sequences against the NCBI RefSeq fungi database using BLAST nucleotide search. BLAST results were
153 filtered using minimum sequence identity thresholds of 60% for primers and 85% for probes. Cross-reactive
154 organisms were identified as those showing significant hits to both primers (aT_F and aT_R) and at least one
155 species-specific probe (Pn_FAM or Ptr_HEX), representing potential targets for non-specific dPCR
156 amplification (Figure 1D). Primers and probe specificity were tested *in vitro* using the ddPCR assay (Figure
157 2C) against the purified gDNA of closely related fungal pathogens and wheat (Table S2).
158
159 ***Biomass Modelling***
160 To approximate a relationship between dPCR copy number and fungal biomass, we developed a two-step
161 calibration approach. First, we quantified the DNA yield per unit fungal tissue by extracting DNA from known
162 quantities of freeze-dried mycelium. Three biological replicates of *P. nodorum* SN15 and *P. tritici-repentis*
163 M4 mycelia were weighed out in technical triplicates between 0.15 and 15 mg and DNA was extracted as
164 described above. Total DNA content was plotted as a function of tissue mass and analysed using linear
165 regression to derive the species-specific DNA-to-tissue ratio (β) for each pathogen. Second, we established
166 the relationship between DNA input and dPCR target copy number by analysing serial dilutions of gDNA
167 from both species. Triplicate samples at concentrations ranging from 0.05 to 500 pg/µl were analysed using
168 the dPCR assay described above. The integrated biomass model combines these relationships through the
169 formula below where C represents dPCR-detected alpha-tubulin copies/µl, α is the target copies per
170 nanogram of DNA, and β is the micrograms of DNA per milligram of tissue. After substituting the
171 experimentally derived values, we obtained simplified predictive equations for each species that enable
172 direct conversion of dPCR-measured target copies into estimated fungal biomass.
173
174 $$Tissue_{(ug)} = \frac{C}{\alpha\beta}$$

175

176 ***Field Sites and Experimental Design***

177 Symptomatic leaf tissue was collected between May and October of 2022 from field sites sown in early April
178 in Western Australia. The first, a disease nursery unattenuated by fungicide for more than ten years
179 (Northam, 31°32'23.4"S 116°42'17.3"E). The second plot (South Perth, -31.991046, 115.888172), contained
180 three adjacent plots, established by incorporating infected wheat stubble containing single or mixed
181 pathogen species into the soil prior to sowing, with cross-contamination between adjacent plots expected
182 over the growing season to test competitive dynamics under varying establishment priorities (Figure S2).
183 Cultivars were selected for resistance through Department of Primary Industries and Regional Development
184 of Western Australia wheat variety disease ratings to select lines with differential susceptibility to SNB and
185 TS (Table 2). SVS (susceptible-very susceptible) indicates wheat cultivars with minimal disease resistance,
186 while MRMS (Moderately Resistant-Moderately Susceptible) denotes cultivars with intermediate resistance
187 levels. Samples were photographed on site, trimmed with a scalpel to 50 mm in length, then stored on ice
188 for ≤ 24h before snap freezing and storage at -80°C until processing.

189

190 ***Attached Leaf Assay***

191 Wheat seedlings were grown under white light on a 12hr photoperiod until 12 days old. Leaves were
192 mounted adaxial side up onto 45mm XPS foam boards using micropore tape inside a seedling tray. Attached
193 leaves were inoculated with 15µl of either $1x10^7$ spores.ml^{-1} of *P. nodorum* SN15 spores, $1x10^5$spores.ml^{-1} of
194 *P. tritici-repentis* M4 spores suspended in 0.02% Tween 20 or a mixture of the two maintaining the original
195 concentration. Following inoculation spore suspension was spread with a paintbrush (WestArt, 4mm
196 Synthetic), leaves allowed to dry, then sealed inside humidity chambers and maintained at 22C ± 1C, ≥ 95%
197 humidity under white light on a 12 hr photoperiod. Staggered infections were carried out 72 hrs post-initial
198 inoculation following the same procedure. Leaves were photographed seven days after secondary infection,
199 before excising a 50mm section with a sterile scalpel.

200

201 ***Statistical analysis***

202 Statistical analyses were performed using R version 4.5.0 [41]. Linear regression analysis was conducted using
203 the lm() function to fit a linear model. Pathogen biomass data were natural log-transformed [ln(biomass +
204 1)] to meet ANOVA assumptions of normality and homogeneity of variance [42] . For field data, Two-way
205 ANOVA was conducted for each site with pathogen presence and wheat line as respective factors. For
206 sequential inoculation data, Two-way ANOVA was conducted for all data with treatment and wheat line as
207 factors. Post-hoc comparisons used Tukey's HSD test when significant effects were detected ($p < 0.05$). All
208 assumptions were verified through residual analysis and Shapiro-Wilk tests for normality.

209

210 **Results**

211 ***Biomass modelling and absolute pathogen DNA quantification using dPCR***

212 To identify a suitable locus for marker development, gene annotations from SN15 and M4 were compared
213 using reciprocal BLAST analysis to identify highly conserved orthologues. Candidates were filtered manually
214 to identify regions ≤200 bp with conserved 5' and 3' termini for primer binding sites adjacent to a divergent
215 central region for a species-specific probe, before selecting a region spanning the final intron of the alpha-
216 tubulin ortholog in both species (Pn_SN15_01762, Ptr_M4_98590). Suitable loci within the orthologous
217 alpha-tubulin coding sequences were identified so that a single primer set could target binding sites
218 conserved across both species, while species-specific internal probes (Pn_FAM and Ptr_HEX respectively)
219 permitted species discrimination (Figure 1A & B). Single copy primer-probe sites were conserved at a single
220 copy across pan-genomes of the respective species, with in silico cross-reactivity analysis confirming
221 minimal risk of in species off target effects (Figure 1C). No cross reactivity to known wheat associated fungi
222 was observed when tested in silico, with only seven primer + probe matches ≤ 98% found excluding target
223 organisms (Figure 1D). Species-specific DNA yield analysis revealed *P. tritici-repentis* produces 0.160 µg
224 DNA per mg dry tissue compared to *P. nodorum* at 0.059 µg DNA per mg dry tissue (Figure 2A). Calibration
225 curves for both probes demonstrated near-perfect linearity ($R^2 > 0.99$) across a broad range of fungal DNA
226 (0.5 $pg.\mu l^{-1}$ to 0.5 $ng.\mu l^{-1}$) for both pathogens (Figure 2B). When tested against gDNA of the wheat host or

227 related fungal species and alternative wheat pathogens, the assay showed no off-target effects (Figure 2C).
228 The integrated biomass model yielded conversion factors of 1.3 µg biomass per target copy for *P. tritici-*
229 *repentis* and 3.4 µg per target copy for *P. nodorum*, providing the foundation for all subsequent comparative
230 analyses (Figure S3).
231

232 ***Incidence of host tissue necrosis (but not chlorosis) correlates with fungal biomass accumulation***

233 Total fungal biomass measured through dPCR correlated with necrosis measured with automatic pixel
234 thresholding (Figure 3A). Controlled infection of wheat cvs Axe and Scepter with single or mixed *P.*
235 *nodorum*/*P. tritici-repentis* inoculum were monitored through photography and tissue sampling over a 10-
236 day post-infection period. Linear regression models were constructed for each of three distinct disease
237 metrics: chlorosis, necrosis and total disease (necrosis plus chlorosis) (Figure 3B). Of the three metrics
238 evaluated, necrosis demonstrated the strongest positive correlation (R^2= 0.705). Total disease coverage
239 (chlorosis plus necrosis) exhibited a moderate positive correlation with pathogen biomass (R^2= 0.445).
240 Interestingly, chlorosis showed a weak negative correlation with pathogen biomass (R^2= 0.214), suggesting
241 that chlorotic symptoms are not indicative of high pathogen loads. We then extended this analysis to
242 naturally infected wheat plants sampled weekly over a 16-week period beginning at tillering stage at a field
243 site. Field data revealed substantial temporal variation in disease-biomass correlations (Figure 3C). Strong
244 correlations similar to controlled conditions were observed in week 1, but collapsed and recovered across
245 the season, likely reflecting temporal confounding as infections at varying stages are sampled
246 simultaneously. This temporal pattern highlighted the importance of assessment timing for the correlation
247 between visual symptom assessment and fungal biomass.
248

249 ***Field co-infection facilitates biomass accumulation and the breakdown of host resistance***

250 Pathogen biomass responses to genetic resistance in host plants were examined in four wheat cultivars with
251 combinatorial differences in TS and SNB disease resistance ratings (Table 1), sampled in a naturally wheat-

252 disease nursery endemic for both *P. nodorum* and *P. tritici-repentis*. Co-infected samples were the most
253 common type observed (63%) validating previous observations [6,16], with single infections representing 21%
254 and 16% of samples for *P. tritici-repentis* and *P. nodorum,* respectively (Figure 4). For Axe (SVS to both TS and
255 SNB), no significant differences in necrosis severity were observed between co-infected and single-infected
256 samples, with significantly higher *P. tritici-repentis* but not *P. nodorum* biomass observed under co-
257 infection. With Emu Rock and Yitpi, the only significant difference observed was a higher proportion of *P.*
258 *nodorum* biomass in Emu Rock, with no single infections of a given pathogen observed in hosts with a
259 resistance to said pathogen.
260
261 Wheat cv. Scepter, which is rated MRMS to both TS and SNB, demonstrated greater necrosis when both
262 pathogens were present (Figure 4A). Both *P. tritici-repentis* and *P. nodorum* were detected at very low single-
263 infection frequencies and significantly less biomass than co-infected samples. In general, both pathogens
264 exhibited significantly higher biomass accumulation under co-infection conditions compared to single-
265 pathogen infections (Figures 4B & C). Notably, the only wheat cultivar to exhibit higher necrosis and biomass
266 during co-infection was Scepter, the host with the highest resistance to both pathogens.
267
268 ***Fair weather friends: P. tritici-repentis facilitates co-infection while P. nodorum suppresses***
269 We sought to isolate priority effects in the field by using a defined primary inoculum in a field trial involving
270 three adjacent plots, capable of spreading airborne inoculum for secondary infections. Exterior plots
271 contained either stubble infected with *P. tritici-repentis* or *P. nodorum* and the central plot contained stubble
272 with an equal mixture of both (Figure S2). For the *P. tritici-repentis* and mixed stubble site, co-infection was
273 again ubiquitous throughout the growing season, suggesting the presence of secondary airborne inoculum
274 [7]. Disease incidences measured by necrosis and biomass for both species were significantly higher under
275 co-infection than for single infection, with the exception of *P. nodorum* at the mixed site, broadly reflecting
276 the patterns seen under endemic conditions (Figures 5, S4 and S5).
277

278 The *P. nodorum* inoculum site revealed dramatically different interaction dynamics. *P. tritici-repentis* failed
279 to establish single-pathogen infection and was only observed at a low frequency in co-infected samples
280 (Figures 5 and S6). This suggests that *P. nodorum* may antagonise secondary *P. tritici-repentis* host-infection
281 indicating priority effects in the tripartite *P. nodorum*-*P. tritici-repentis*-wheat.
282
283 ***Controlled sequential infection reveals an asymmetric partnership***
284 To confirm this antagonism, we conducted sequential co-infection assays to investigate the role of temporal
285 dynamics. *P. nodorum* and *P. tritici-repentis* were inoculated onto wheat cvs. Axe and Scepter seedlings in
286 a controlled environmental growth chamber, where secondary infection was carried out 72 hrs after primary
287 infection using defined pathogen isolates. Analysis of wheat cv. Axe revealed consistent biomass
288 accumulation and necrosis development across treatments as well as secondary-infection timings (Figure
289 6A). Simultaneous inoculation resulted in *P. tritici-repentis* dominance, while *P. tritici-repentis* priority led to
290 balanced pathogen loads with no significant competitive advantage for either species pertaining to biomass
291 accumulation. When *P. nodorum* was applied as a primary inoculum ahead of *P. tritici-repentis*, it again
292 inhibited subsequent *P. tritici-repentis* biomass accumulation. This was the strongest competitive
293 asymmetry observed across all treatments on wheat cv. Axe and provides additional evidence of the
294 inhibitory dynamics observed under field conditions.
295
296 Sequential co-infection on wheat cv. Scepter displayed markedly different infection dynamics. Most
297 treatments resulted in substantially reduced pathogen biomass and necrosis compared to wheat cv Axe,
298 likely due to background resistance (Figure 6B). *P. tritici-repentis* followed by *P. nodorum* inoculation was
299 the sole exception, representing a breakdown of seedling resistance where both pathogens achieved
300 biomass levels comparable to those in susceptible plants. This treatment was also the only one to induce
301 significant necrosis in resistant plants, suggesting that *P. tritici-repentis* establishment compromises
302 subsequent resistance responses to *P. nodorum,* allow both pathogens to proliferate.
303

304 Collectively, this work confirms priority effects influence pathogen proliferation in the SNB-TS/wheat
305 pathosystem. Under natural field conditions, co-infection is ubiquitous and facilitates biomass
306 accumulation for both pathogens, synergistically break down host resistance. When the inoculum source
307 is controlled, *P. nodorum* suppresses *P. tritici-repentis* establishment, while *P. tritici-repentis* facilitates
308 balanced co-infection. In controlled sequential infections, *P. tritici-repentis* primacy enables both
309 pathogens to overcome genetic resistance, while *P. nodorum* primary infection consistently suppresses *P.*
310 *tritici-repentis* infection regardless of host background.
311

312 **Discussion**

313 Co-infection dynamics play crucial roles in wheat pathosystems, affecting pathogen virulence and
314 epidemiology. Priority effects have been shown to impact disease development and competitive advantage
315 [43], immune suppression enabling persistence of normally avirulent strains [44], and effector complementation
316 between strains enhancing disease severity [45]. The challenge of accurately measuring pathogen abundance
317 in polymicrobial leaf spot diseases has been well established prior to this study [24,25]. Previous studies using
318 RT-PCR were able to highlight the high frequency of wheat co-infection by *P. nodorum* and *P. tritici-repentis*,
319 however the work was limited by available technology to measuring relative pathogen abundance [6,27,28].
320

321 Our methods represent a significant advancement in the study of polymicrobial plant diseases. Through
322 species-specific DNA yield normalization, we showed *P. tritici-repentis* yielded almost three times the DNA
323 per milligram of tissue compared to *P. nodorum*. Using a conserved single copy gene eliminates variability
324 between strains while the utilization of dPCR retains sufficient sensitivity for field applications. This provided
325 a strong foundation to investigate the relationship pathogen abundance and visual symptoms, wheat
326 cultivar disease resistance ratings, and the role of priority effects in the outcome of disease. Our findings
327 reveal two interactions. The first is co-operative, where *P. tritici-repentis* priority establishment facilitates
328 subsequent *P. nodorum* colonisation and enhances disease severity and biomass for both pathogens in a
329 resistant host . The second is competitive, where *P. nodorum* priority establishment suppresses *P. tritici-*

330 *repentis* colonisation regardless of host resistance background. To our knowledge, this is the first study to
331 observe asymmetric facilitation overcoming host resistance in a fungal plant pathosystem.
332
333 Field trials where *P. tritici-repentis* was introduced first reproduced facilitation patterns observed in naturally
334 infected fields. Priority establishment by *P. tritici-repentis* may drive the co-infection observed in wheat
335 production systems, where *P. tritici-repentis* ascospores have been shown to mature up to three months
336 before those of *P. nodorum* in south-west Western Australia [46,47]. In addition, *P. tritici-repentis* may benefit
337 from superior establishment characteristics, including larger resource-rich and temperature-resistant
338 conidia [48,49]. When *P. tritici-repentis* establishes on resistant host leaves it facilitates *P. nodorum* colonisation
339 leading to greater disease through an unknown mechanism that leads positive interference where temporal
340 sequence determines resistance breakdown. *Zymoseptoria tritici* followed by *Pseudomonas syringae*
341 infection leads to systemically induced bacterial susceptibility in wheat, where fungal infection facilitates
342 colonization through suppression of immune-related metabolites [50]. Priority effects may exploit depleted
343 immune responses, where initial infection activates energetically costly defence signalling pathways
344 creating windows of vulnerability for secondary infections [51]. Necrotrophic pathogens can subvert plant
345 defence responses that evolved primarily against biotrophic pathogens including the salicylic acid pathway,
346 which while providing resistance against biotrophs, can enhance susceptibility to necrotrophs [52].
347
348 Necrotrophic pathogens create favourable conditions for subsequent colonisation by generating necrotic
349 lesions with effectors that cause necrosis and provide nutrient-rich substrates from lysed plant cells,
350 support necrotrophic growth [53]. Our observations are distinguished by the asymmetric nature of this
351 facilitation despite both pathogens producing necrotrophic effectors infection on wheat [14,39]. This suggests
352 that mechanistic differences beyond necrotrophic virulence determine the facilitative outcomes we
353 observed. Previously, *P. nodorum* strains producing high levels of necrotrophic effectors rescued reduced
354 virulence strains on susceptible wheat, maintaining overall virulence of the pathogen population [45]. Similarly
355 the introduction reduced virulence mutants of *Magnaporthe oryzae* into populations of wild-type strains

356 resulted in enhanced overall population fitness and increased damage to rice hosts [11]. These examples
357 illustrate that cooperation between pathogen strains with different virulence capabilities can lead to
358 enhanced disease outcomes, representing a distinct mechanism from host immune suppression-
359 mediated facilitation. The mechanism underlying the facilitation observed in our data remains unclear, but
360 could involve direct pathogen-pathogen interactions, host immune suppression, or both processes working
361 in combination [9].
362
363 *P. nodorum* priority establishment antagonises *P. tritici-repentis* colonisation across all host genotypes
364 observed in the field and laboratory, suggesting a physiological mechanism possessed by *P. nodorum* to
365 suppress the growth of competitors. While *P. nodorum* and *P. tritici-repentis* share a near-identical ToxA [19],
366 *P. nodorum* possesses a diverse collection of characterised necrotrophic effectors including SnTox1,
367 SnTox3, SnTox5 [54]and SnTox267 [55]. *Verticillium dahliae* has co-opted antimicrobial proteins specifically for
368 manipulating fungal competitors during host colonization [56], suggesting exclusion through biochemical
369 interference may be an evolved strategy rather than an incidental consequence of infection. It is not known
370 if characterised *P. nodorum* NEs possess antimicrobial functions however, SnTox1 possess dual functions;
371 facilitating necrosis in wheat and binding chitin, possibly to evade host PAMP-triggered recognition [57]. Recent
372 pan-genomic analysis of *P. nodorum* identified an abundance of candidate secreted effector proteins,
373 including numerous homologs to known antimicrobial effectors from other fungal species [38]. In addition, *P.*
374 *nodorum* possesses an extensive arsenal of secondary metabolite biosynthesis genes [58]. Previous studies
375 revealed that *P. nodorum* was capable of producing volatile organic compounds that exhibit phytotoxic and
376 antimicrobial activities [49,59,60]. It remains to be seen if these secondary metabolites possess bioactivity that
377 antagonises *P. tritici-repentis* [61].
378
379 Molecular quantification revealed competitive exclusion patterns masked by visual assessment. While
380 necrosis provides a reliable estimate of total pathogen biomass under controlled conditions, visual
381 symptoms cannot reliably distinguish between single and co-infection states. Additionally, quantification of

382 disease can be hindered by simultaneous biotic and abiotic stresses, emphasising the need for molecular
383 approaches that quantify pathogens biomass [62]. Even with automated image analysis tools like LeafScan,
384 which can accurately quantify necrotic tissue area, morphologically indistinguishable lesions produced by
385 *P. nodorum* and *P. tritici-repentis* provide no visual indication of their microbial composition. The correlation
386 observed under controlled infection suggests that both pathogens primarily colonise necrotic tissue
387 regions, likely secreting necrotrophic effectors into surrounding tissue to induce chlorosis ahead of
388 colonisation, supporting previous mechanistic studies [63].
389
390 These sequence-dependent interactions represent a form of historical contingency where early colonisers
391 fundamentally alter the trajectory of microbial community development within host tissues [1]. The facilitative
392 and competitive mechanisms we observed demonstrate that pathogen communities are not simply
393 assembled through independent colonisation events, but rather through complex ecological networks
394 where arrival order determines interaction outcomes [5]. This challenges traditional views of agricultural
395 pathosystems as simplified host-pathogen dyads and instead positions them as dynamic microbial
396 ecosystems governed by community assembly rules similar to those operating in natural systems [2], but with
397 accelerated temporal dynamics due to the intensive selection pressures of agricultural environments [3].
398 Agricultural monocultures may thus serve as model systems for understanding rapid microbial community
399 assembly processes under simplified environmental conditions, offering insights into fundamental
400 ecological principles that operate across diverse ecosystems while providing practical applications for
401 sustainable disease management strategies.

402 Several priorities emerge from this work. We recommend that future disease resistance trials of commercial
403 wheat cultivars consider rating for the SNB-TS complex over the current single disease resistance rating
404 system in wheat-growing regions where *P. nodorum* and *P. tritici-repentis* are endemic. Furthermore,
405 additional analysis of the effect that co-infection may have on grain yields is needed. Field validation studies
406 across diverse environments and wheat genetic backgrounds are needed to determine the generalisability

of our sequence-dependent findings, particularly investigating whether similar priority effects occur in cultivars with different resistance backgrounds.

Acknowledgements

The authors would like to thank; Noel Knight (Curtin University) and Lincoln Harper (Curtin University) for assistance with dPCR assay design; Julie Lawrence (Curtin University) and Manisha Shankar (DPIRD) for providing off-target isolates for dPCR validation. We extend our thanks to Dr Araz Abdullah (Curtin University) for insightful discussions and for establishing the precursor groundwork for this study. This study was conducted by the Centre for Crop and Disease Management, a co-investment between the Grains Research and Development Corporation (GRDC) and Curtin University - grant CUR1403-002BLX.

Data Accessibility Statement

All data supporting the results of this study are available as follows: Raw dPCR data, image analysis outputs, and statistical analysis code are archived in the Dryad Digital Repository at [DOI to be provided upon acceptance]. The LeafScan image processing and analysis tools are freely available at https://github.com/LeonLenzo/leaf-scan. Reference genome assemblies for *Parastagonospora nodorum* SN15 and *Pyrenophora tritici-repentis* M4 are publicly available through NCBI GenBank. Primer and probe sequences for the duplex dPCR assay are provided in the Materials and Methods section. Field sampling coordinates and experimental metadata are included in the supplementary materials. All materials and protocols are available upon reasonable request to the corresponding author.

References

1. Fukami T. Historical Contingency in Community Assembly: Integrating Niches, Species Pools, and Priority Effects. *Annu. Rev. Ecol. Evol. Syst.* 2015 **46**:1–23. https://doi.org/10.1146/annurev-ecolsys-110411-160340.

2. Vacher C, A Hampe, AJ Porté, et al. The Phyllosphere: Microbial Jungle at the Plant-Climate Interface. *Annu. Rev. Ecol. Evol. Syst.* 2016 **47**:1–24. https://doi.org/10.1146/annurev-ecolsys-121415-032238.

3. McDonald BA, EH Stukenbrock. Rapid emergence of pathogens in agro-ecosystems: global threats to agricultural sustainability and food security. *Philos. Trans. R. Soc. B Biol. Sci.* 2016 **371**. https://doi.org/10.1098/rstb.2016.0026.

4. Halliday FW, RM Penczykowski, B Barrès, et al. Facilitative priority effects drive parasite assembly under coinfection. *Nat. Ecol. Evol.* 2020 **4**:1510–21. https://doi.org/10.1038/s41559-020-01289-9.

5. Debray R, RA Herbert, AL Jaffe, et al. Priority effects in microbiome assembly. *Nat. Rev. Microbiol.* 2022 **20**:109–21. https://doi.org/10.1038/s41579-021-00604-w.

6. Fejer Justesen A, B Corsi, A Ficke, et al. Hidden in plain sight: a molecular field survey of three wheat leaf blotch fungal diseases in North-Western Europe shows co-infection is widespread. *Eur. J. Plant Pathol.* 2021 **160**:949–62. https://doi.org/10.1007/S10658-021-02298-5.

7. Van der Heyden H, P Dutilleul, J-B Charron, et al. Monitoring airborne inoculum for improved plant disease management. A review. *Agron. Sustain. Dev.* 2021 **41**:40–40. https://doi.org/10.1007/s13593-021-00694-z.

8. Ferreira RBR, LCM Antunes, N Sal-Man. Pathogen-pathogen interactions during co-infections. *ISME J.* 2025 **19**:wraf104. https://doi.org/10.1093/ismejo/wraf104.

9. Dutt A, D Andrivon, C Le May. Multi-infections, competitive interactions, and pathogen coexistence. *Plant Pathol.* 2022 **71**:5–22. https://doi.org/10.1111/ppa.13469.

10. Harrison F, LE Browning, M Vos, et al. Cooperation and virulence in acute Pseudomonas aeruginosa infections. *BMC Biol.* 2006 **4**:21. https://doi.org/10.1186/1741-7007-4-21.

11. Lindsay RJ, MJ Kershaw, BJ Pawlowska, et al. Harbouring public good mutants within a pathogen population can increase both fitness and virulence. *eLife* 2016 **5**:e18678. https://doi.org/10.7554/eLife.18678.

12. Mousa WK, A Schwan, J Davidson, et al. An endophytic fungus isolated from finger millet (Eleusine coracana) produces anti-fungal natural products. *Front. Microbiol.* 2015 **6**:1157. https://doi.org/10.3389/fmicb.2015.01157.

13. Orton ES, JKM Brown. Reduction of growth and reproduction of the biotrophic fungus Blumeria graminis in the presence of a necrotrophic pathogen. *Front. Plant Sci.* 2016 **7**:742–742. https://doi.org/10.3389/FPLS.2016.00742/BIBTEX.

14. Gourlie R, M McDonald, M Hafez, et al. The pangenome of the wheat pathogen Pyrenophora tritici-repentis reveals novel transposons associated with necrotrophic effectors ToxA and ToxB. *BMC Biol.* 2022 **20**. https://doi.org/10.1186/s12915-022-01433-w.

15. McDonald BA. How knowledge of pathogen population biology informs management of Septoria nodorum blotch on wheat. *Eur. J. Plant Pathol.* 2025 **171**:531–45. https://doi.org/10.1007/s10658-024-02996-w.

16. Abdullah AS, MR Gibberd, J Hamblin. Co-infection of wheat by Pyrenophora tritici-repentis and Parastagonospora nodorum in the wheatbelt of Western Australia. *Crop Pasture Sci.* 2020 **71**:119–27. https://doi.org/10.1071/CP19412.

17. Möller M, EH Stukenbrock. Evolution and genome architecture in fungal plant pathogens. *Nat. Rev. Microbiol.* 2017 **15**:756–71. https://doi.org/10.1038/nrmicro.2017.76.

18. McDonald MC, PS Solomon. Just the surface: advances in the discovery and characterization of necrotrophic wheat effectors. *Curr. Opin. Microbiol.* 2018 **46**:14–8. https://doi.org/10.1016/J.MIB.2018.01.019.

19. Friesen TL, EH Stukenbrock, Z Liu, et al. Emergence of a new disease as a result of interspecific virulence gene transfer. *Nat. Genet. 2006 388* 2006 **38**:953–6. https://doi.org/10.1038/ng1839.

20. Vleeshouwers VGAA, RP Oliver. Effectors as tools in disease resistance breeding against biotrophic, hemibiotrophic, and necrotrophic plant pathogens. *Mol. Plant. Microbe Interact.* 2014 **27**:196–206. https://doi.org/10.1094/MPMI-10-13-0313-IA.

21. Francki MG, E Walker, CJ McMullan, et al. Multi-Location Evaluation of Global Wheat Lines Reveal Multiple QTL for Adult Plant Resistance to Septoria Nodorum Blotch (SNB) Detected in Specific Environments and in Response to Different Isolates. *Front. Plant Sci.* 2020 **11**. https://doi.org/10.3389/fpls.2020.00771.

22. Shankar M, D Mather, H Golzar, et al. *Stacking yellow spot resistance genes into fixed lines results in genetic gain*. 2015. https://www.researchgate.net/publication/305748820.

23. Peters Haugrud AR, G Shi, S Seneviratne, et al. Genome-wide association mapping of resistance to the foliar diseases septoria nodorum blotch and tan spot in a global winter wheat collection. *Mol. Breed. New Strateg. Plant Improv.* 2023 **43**:54. https://doi.org/10.1007/s11032-023-01400-5.

24. Beard C, G Thomas, A Hills, et al. *Yellow spot and septoria nodorum blotch and their management in wheat*. 2024. https://library.dpird.wa.gov.au/fc_factsheets/70.

25. Friskop A, Z Liu. *Fungal Leaf Spot Diseases of Wheat: Tan spot, Septoria/Stagonospora nodorum blotch and Septoria tritici blotch (PP1249)*. 2021. www.ag.ndsu.edu/extension.

26. Long M, M Hartley, RJ Morris, et al. Classification of wheat diseases using deep learning networks with field and glasshouse images. *Plant Pathol.* 2023 **72**:536–47. https://doi.org/10.1111/ppa.13684.

27. Abdullah AS, C Turo, CS Moffat, et al. Real-time PCR for diagnosing and quantifying co-infection by two globally distributed fungal pathogens of wheat. *Front. Plant Sci.* 2018 **9**:1086–1086. https://doi.org/10.3389/FPLS.2018.01086/BIBTEX.

28. Fu H, J Jiang, MW Harding, et al. Development of a triplex qPCR system for the detection of Parastagonospora nodorum, Zymoseptoria tritici and Pyrenophora tritici-repentis from wheat. *Plant Dis.* 2025. https://apsjournals.apsnet.org/doi/10.1094/PDIS-01-25-0003-SR (18 August 2025, date last accessed).

29. Moffat CS, PT See, RP Oliver. Leaf yellowing of the wheat cultivar Mace in the absence of yellow spot disease. *Australas. Plant Pathol.* 2015 **44**:161–6. https://doi.org/10.1007/s13313-014-0335-2.

30. Hall AT, AM Zovanyi, DR Christensen, et al. Evaluation of Inhibitor-Resistant Real-Time PCR Methods for Diagnostics in Clinical and Environmental Samples. *PLOS ONE* 2013 **8**:e73845. https://doi.org/10.1371/journal.pone.0073845.

31. Huggett JF, CA Foy, V Benes, et al. The digital MIQE guidelines: Minimum information for publication of quantitative digital PCR experiments. *Clin. Chem.* 2013 **59**:892–902. https://doi.org/10.1373/clinchem.2013.206375.

32. Solomon PS, SW Thomas, P Spanu, et al. The utilisation of di/tripeptides by Stagonospora nodorum is dispensable for wheat infection. *Physiol. Mol. Plant Pathol.* 2003 **63**:191–9. https://doi.org/10.1016/j.pmpp.2003.12.003.

33. Moolhuijzen P, PT See, CS Moffat. A new PacBio genome sequence of an Australian Pyrenophora tritici-repentis race 1 isolate. *BMC Res. Notes* 2019 **12**:642–642. https://doi.org/10.1186/s13104-019-4681-6.

34. Rybak K, PT See, HTT Phan, et al. A functionally conserved Zn2Cys6 binuclear cluster transcription factor class regulates necrotrophic effector gene expression and host-specific virulence of two major Pleosporales fungal pathogens of wheat. *Mol. Plant Pathol.* 2017 **18**:420–34. https://doi.org/10.1111/mpp.12511.

35. Liu ZH, JD Faris, SW Meinhardt, et al. Genetic and physical mapping of a gene conditioning sensitivity in wheat to a partially purified host-selective toxin produced by Stagonospora nodorum. *Phytopathology* 2004 **94**:1056–60.

36. Jacques S, L Lenzo, K Stevens, et al. An optimized sporulation method for the wheat fungal pathogen Pyrenophora tritici-repentis. *Plant Methods* 2021 **17**:52–52. https://doi.org/10.1186/s13007-021-00751-4.

37. Abràmoff MD, PJ Magalhães, SJ Ram. Image processing with ImageJ. *Biophotonics Int.* 2004 **11**:36–42.

38. Jones DAB, K Rybak, M Hossain, et al. Repeat-induced point mutations driving Parastagonospora nodorum genomic diversity are balanced by selection against non-synonymous mutations. *Commun. Biol.* 2024 **7**:1614. https://doi.org/10.1038/s42003-024-07327-7.

39. Syme RA, K-C Tan, K Rybak, et al. Pan-Parastagonospora comparative genome analysis—effector prediction and genome evolution. *Genome Biol. Evol.* 2018 **10**:2443–57.
40. Moolhuijzen PM, PT See, G Shi, et al. A global pangenome for the wheat fungal pathogen Pyrenophora tritici-repentis and prediction of effector protein structural homology. *Microb. Genomics* 2022 **8**:mgen000872. https://doi.org/10.1099/mgen.0.000872.
41. R Core Team. R: A Language and Environment for Statistical Computing. 2025.
42. Keene ON. The log transformation is special. *Stat. Med.* 1995 **14**:811–9. https://doi.org/10.1002/sim.4780140810.
43. Suffert F, G Delestre, F Carpentier, et al. Fashionably late partners have more fruitful encounters: Impact of the timing of co-infection and pathogenicity on sexual reproduction in Zymoseptoria tritici. *Fungal Genet. Biol.* 2016 **92**:40–9. https://doi.org/10.1016/J.FGB.2016.05.004.
44. Barrett LG, M Zala, A Mikaberidze, et al. Mixed infections alter transmission potential in a fungal plant pathogen. *Environ. Microbiol.* 2021 **23**:2315–30. https://doi.org/10.1111/1462-2920.15417.
45. John E, S Jacques, HTT Phan, et al. Variability in an effector gene promoter of a necrotrophic fungal pathogen dictates epistasis and effector-triggered susceptibility in wheat. *PLOS Pathog.* 2022 **18**:e1010149.
46. Bathgate JA, R Loughman. Ascospores are a source of inoculum of Phaeosphaeria nodorum, P. Avenaria f. sp. Avenaria and Mycosphaerella graminicola in Western Australia. *Australas. Plant Pathol.* 2001 **30**:317–22. https://doi.org/10.1071/AP01043.
47. Galloway J, M Salam, P Payne. *Less yellow spot in wheat: progress towards a decision support tool that will predict when yellow spot spores are released from the previous season stubble*. 2016.
48. Benslimane H, S Aouali, A Khalfi, et al. In vitro morphological characteristics of Pyrenophora tritici-repentis isolates from several Algerian agro-ecological zones. *Plant Pathol. J.* 2017 **33**:109–17. https://doi.org/10.5423/PPJ.OA.09.2015.0189.
49. Muria-Gonzalez MJ, Y Yeng, S Breen, et al. Volatile Molecules Secreted by the Wheat Pathogen Parastagonospora nodorum Are Involved in Development and Phytotoxicity. *Front. Microbiol.* 2020 **11**. https://doi.org/10.3389/fmicb.2020.00466.
50. Seybold H, TJ Demetrowitsch, MA Hassani, et al. A fungal pathogen induces systemic susceptibility and systemic shifts in wheat metabolome and microbiome composition. *Nat. Commun.* 2020 **11**. https://pubmed.ncbi.nlm.nih.gov/32313046/.
51. Balint-Kurti P. The plant hypersensitive response: concepts, control and consequences. *Mol. Plant Pathol.* 2019 **20**:1163–78. https://doi.org/10.1111/MPP.12821.
52. Glazebrook J. Contrasting mechanisms of defense against biotrophic and necrotrophic pathogens. *Annu. Rev. Phytopathol.* 2005 **43**:205–27. https://doi.org/10.1146/annurev.phyto.43.040204.135923.
53. Tan KC, RP Oliver. Regulation of proteinaceous effector expression in phytopathogenic fungi. *PLoS Pathog.* 2017 **13**. https://pubmed.ncbi.nlm.nih.gov/28426760/.
54. Kariyawasam GK, JK Richards, NA Wyatt, et al. The Parastagonospora nodorum necrotrophic effector SnTox5 targets the wheat gene Snn5 and facilitates entry into the leaf mesophyll. *New Phytol.* 2022 **233**:409–26. https://doi.org/10.1111/nph.17602.
55. Richards JK, GK Kariyawasam, S Seneviratne, et al. A triple threat: the Parastagonospora nodorum SnTox267 effector exploits three distinct host genetic factors to cause disease in wheat. *New Phytol.* 2022 **233**:427–42. https://doi.org/10.1111/nph.17601.
56. Snelders NC, GC Petti, GCM van den Berg, et al. An ancient antimicrobial protein co-opted by a fungal plant pathogen for in planta mycobiome manipulation. *Proc. Natl. Acad. Sci.* 2021 **118**:e2110968118–e2110968118. https://doi.org/10.1073/pnas.2110968118.
57. Liu Z, Y Gao, YM Kim, et al. SnTox1, a Parastagonospora nodorum necrotrophic effector, is a dual-function protein that facilitates infection while protecting from wheat-produced chitinases. *New Phytol.* 2016 **211**:1052–64. https://doi.org/10.1111/nph.13959.
58. Chooi YH, MJ Muria-Gonzalez, PS Solomon. A genome-wide survey of the secondary metabolite biosynthesis genes in the wheat pathogen Parastagonospora nodorum. *Mycology* 2014 **5**:192–206. https://doi.org/10.1080/21501203.2014.928386.

696 59. Chooi YH, C Krill, RA Barrow, et al. An In planta-expressed polyketide synthase produces (R)-mellein in
697 the wheat pathogen Parastagonospora nodorum. *Appl. Environ. Microbiol.* 2015 **81**:177–86.
698 https://doi.org/10.1128/AEM.02745-14.
699 60. Chooi YH, G Zhang, J Hu, et al. Functional genomics-guided discovery of a light-activated phytotoxin in
700 the wheat pathogen Parastagonospora nodorum via pathway activation. *Environ. Microbiol.* 2017 **19**:1975–
701 86. https://doi.org/10.1111/1462-2920.13711.
702 61. Robey MT, LK Caesar, MT Drott, et al. An interpreted atlas of biosynthetic gene clusters from 1,000 fungal
703 genomes. *Proc. Natl. Acad. Sci.* 2021 **118**:e2020230118. https://doi.org/10.1073/pnas.2020230118.
704 62. Bock CH, JGA Barbedo, EM Del Ponte, et al. From visual estimates to fully automated sensor-based
705 measurements of plant disease severity: status and challenges for improving accuracy. *Phytopathol. Res.*
706 2020 **2**. https://doi.org/10.1186/s42483-020-00049-8.
707 63. Faris JD, Z Zhang, H Lu, et al. A unique wheat disease resistance-like gene governs effector-triggered
708 susceptibility to necrotrophic pathogens. *Proc. Natl. Acad. Sci.* 2010 **107**:13544–9.
709 https://doi.org/10.1073/pnas.1004090107.
710 64. Shackley B, C Zaicou-Kunesch, H Dhammu, et al. *Wheat Variety Guide for WA Wheat variety guide for*
711 *WA 2014*. 2014.
712 65. Shackley B, D Nicol, J Curry, et al. *Department of Primary Industries and Regional Development Crop*
713 *Sowing Guide 2022*. 2022.
714 66. Bertazzoni S, DAB Jones, HT Phan, et al. Chromosome-level genome assembly and manually-curated
715 proteome of model necrotroph Parastagonospora nodorum Sn15 reveals a genome-wide trove of
716 candidate effector homologs, and redundancy of virulence-related functions within an accessory
717 chromosome. *BMC Genomics* 2021 **22**:382–382. https://doi.org/10.1186/s12864-021-07699-8.
718 67. McDonald MC, AP Taranto, E Hill, et al. Transposon-mediated horizontal transfer of the host-specific
719 virulence protein ToxA between three fungal wheat pathogens. *mBio* 2019 **10**.
720 https://doi.org/10.1128/mBio.01515-19.

721

Figures

A

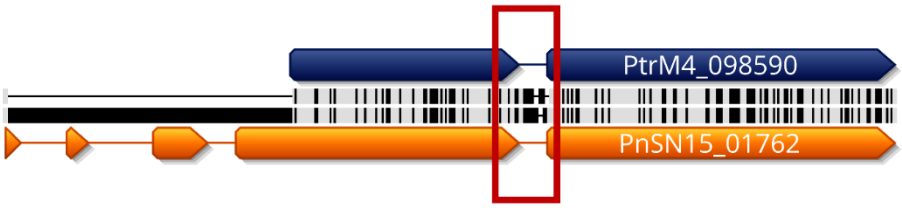
PtrM4_098590
PnSN15_01762

B

aT_F
aT_R
Ptr_HEX
Pn_FAM
A
C
G
T

C

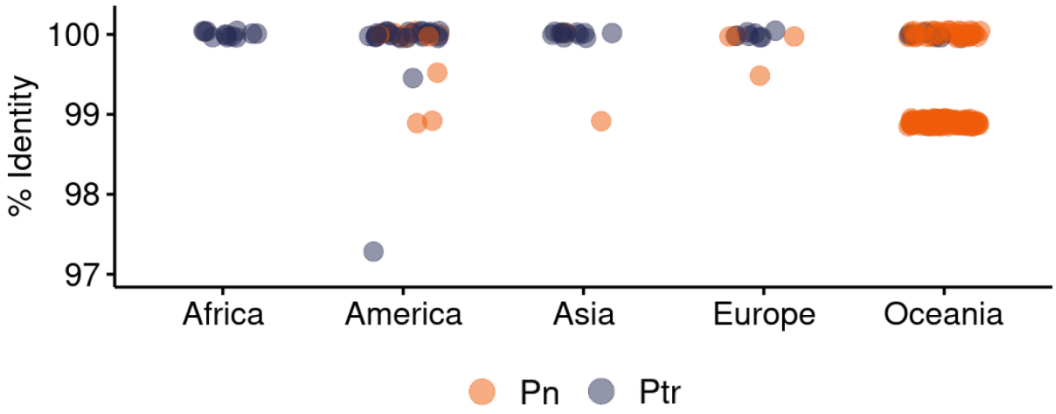
% Identity
100
99
98
97
Africa
America
Asia
Europe
Oceania
Pn
Ptr

D

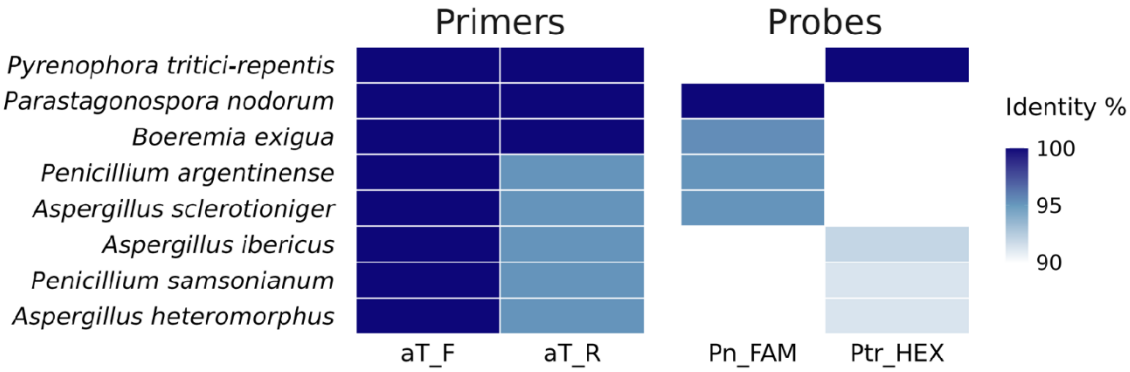
Primers
Probes
Pyrenophora tritici-repentis
Parastagonospora nodorum
Boeremia exigua
Penicillium argentinense
Aspergillus sclerotioniger
Aspergillus ibericus
Penicillium samsonianum
Aspergillus heteromorphus
aT_F
aT_R
Pn_FAM
Ptr_HEX
Identity %
100
95
90

438 ***Figure 1: dPCR Design***

439 **(A)** Pairwise alignment of PnSN15_01762 (Orange) and PtrM4_098590 (Blue), the orthologues for alpha
440 tubulin. Locus aT is highlighted in red. **(B)** Primer and probe design showing aT_F and aT_R amplification
441 primers (green arrows) with species-specific probes Ptr_HEX (blue) and Pn_FAM (orange). Coloured bars
442 indicate sequence polymorphisms. **(C)** Percentage Identity of the aT region across pan-genome
443 assemblies. **(D)** Heatmap showing sequence identity between primer/probe sequences and organisms in
444 the Refseq fungi database.

445

A

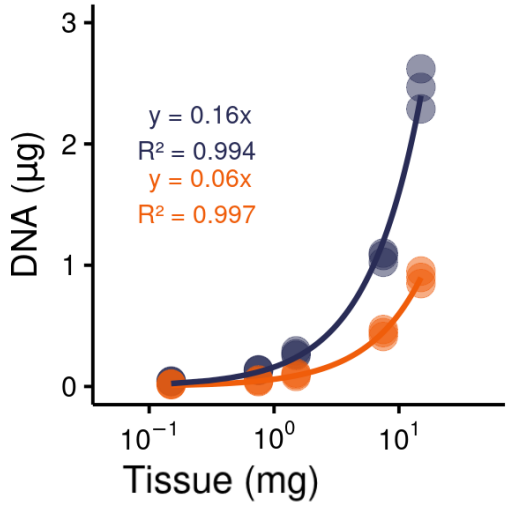
y = 0.16x
R² = 0.994
y = 0.06x
R² = 0.997
DNA (µg)
Tissue (mg)

B

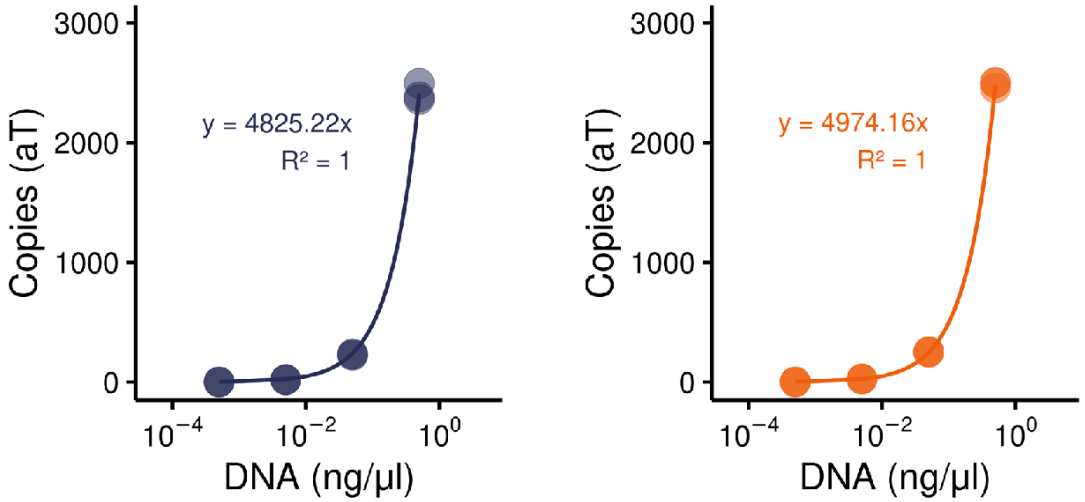
y = 4825.22x
R² = 1
Copies (aT)
DNA (ng/µl)
y = 4974.16x
R² = 1
Copies (aT)
DNA (ng/µl)

C

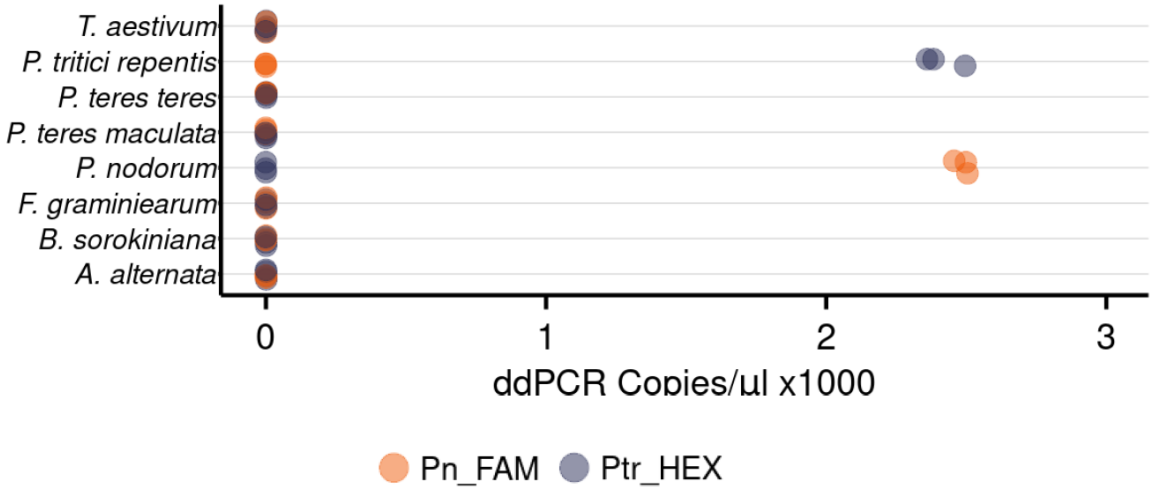
T. aestivum
P. tritici repentis
P. teres teres
P. teres maculata
P. nodorum
F. graminiearum
B. sorokiniana
A. alternata
ddPCR Copies/µl x1000
Pn_FAM
Ptr_HEX

447 ***Figure 2: dPCR Validation***

448 **(A)** Standard curves showing linear relationship (β) between DNA yield for *P. tritici-repentis* (blue) and *P.*
449 *nodorum* (orange). **(B)** Standard curves for Ptr_HEX (blue) and Pn_FAM (orange) probes showing linear
450 relationship (α) between DNA concentration and copy number. **(C)** Specificity testing of the dPCR assay
451 against gDNA from wheat host and related fungal species, showing probe-specific amplification patterns.

452

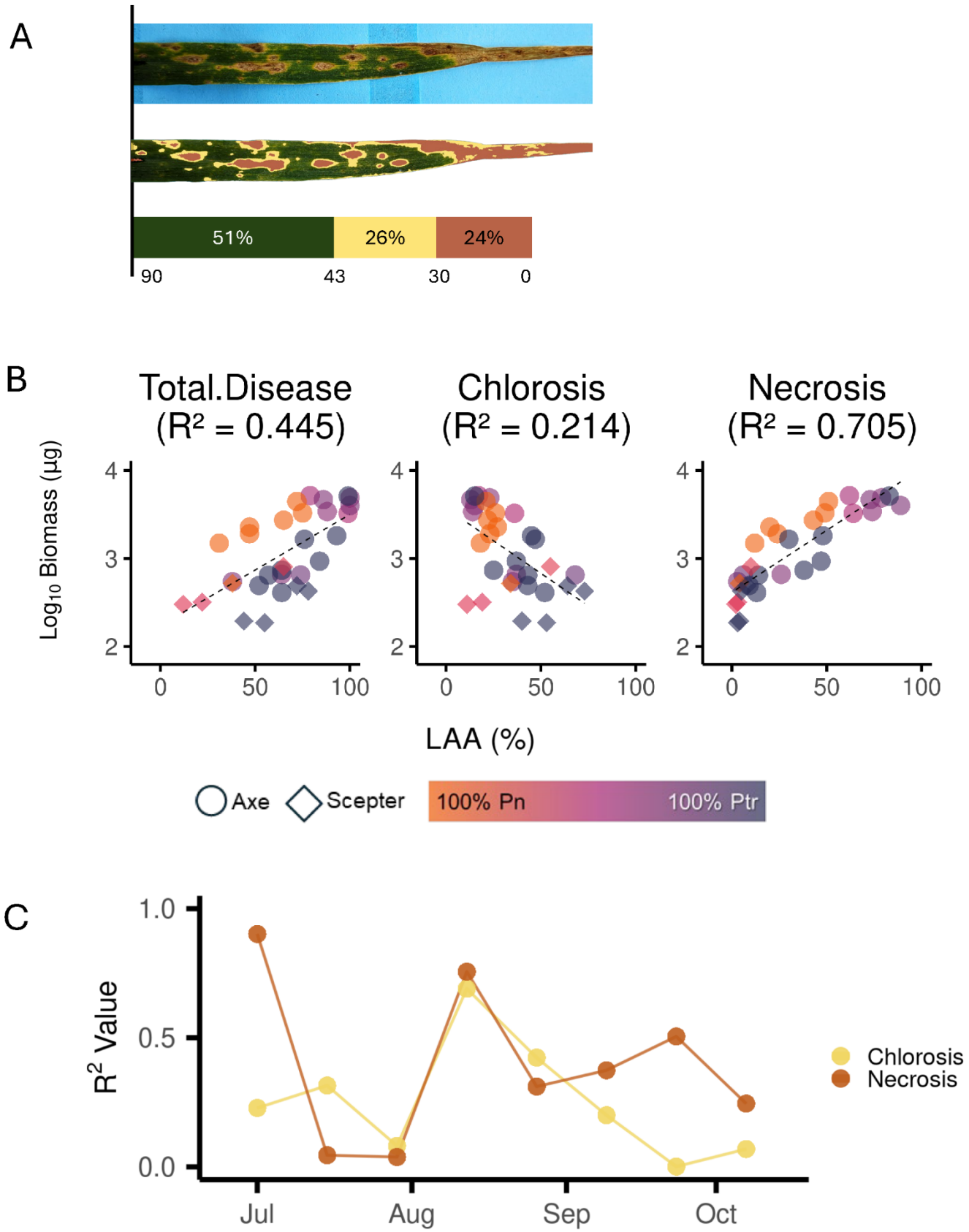
A
51%
26%
24%
90
43
30
0
B
Total.Disease
(R² = 0.445)
Chlorosis
(R² = 0.214)
Necrosis
(R² = 0.705)
Log10 Biomass (µg)
LAA (%)
Axe
Scepter
100% Pn
100% Ptr
C
R2 Value
1.0
0.5
0.0
Jul
Aug
Sep
Oct
Chlorosis
Necrosis

Figure 3: Disease biomass correlation

(A) Automated leaf segmentation showing original image, processed output with disease classification (green = healthy, yellow = chlorotic, brown = necrotic), and HSV hue thresholds. **(B)** Correlations between pathogen biomass and leaf area affected (LAA) by different visual disease metrics. Points represent Axe (susceptible, circles) and Scepter (resistant, diamonds) varieties with single or mixed infections. Colour gradient indicates *P. nodorum* (orange) to *P. tritici-repentis* (blue) proportion. R^2 shows correlation strength for total disease, r shows correlation co-efficient. **(C)** Temporal variation in visual disease-biomass correlations under field conditions over a 16-week sampling period. Lines show R^2 values for chlorosis (yellow), necrosis (brown) metrics.

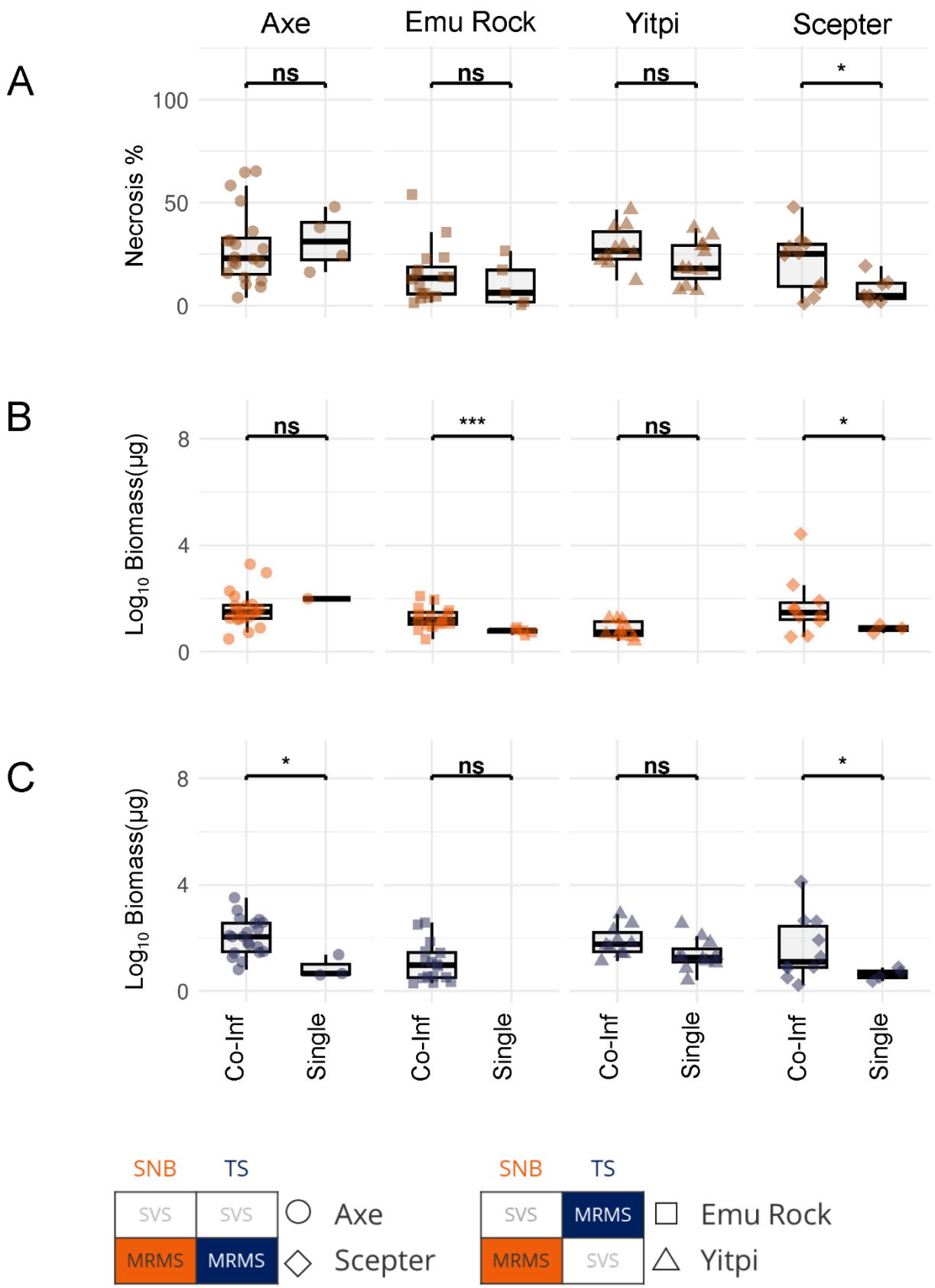
A
B
C
Axe
Emu Rock
Yitpi
Scepter
ns
*
***
Necrosis %
Log10 Biomass(µg)
Co-Inf
Single
SNB
TS
SVS
MRMS
Axe
Scepter
Emu Rock
Yitpi

465 ***Figure 4: Host genetics in natural field disease***

466 **(A)** disease severity (necrosis %, brown), **(B)** *P. nodorum* biomass (orange), and **(C)** *P. tritici-repentis* (blue)

467 biomass across four wheat lines: Axe (SVS to SNB and TS), Emu Rock (SVS to SNB, MRMS to TS), Scepter

468 (MRMS to SNB and TS), and Yitpi (MRMS to SNB SVS to TS). Points represent individual wheat leaves with

469 shapes indicating cultivar (circles = Axe, squares = Emu, diamonds = Scepter, triangles = Yitpi). Statistical

470 significance of differences between co-infection and single infection within each wheat line indicated above

471 brackets (ns = not significant, * $p < 0.05$, ** $p < 0.01$, *** $p < 0.001$).

472

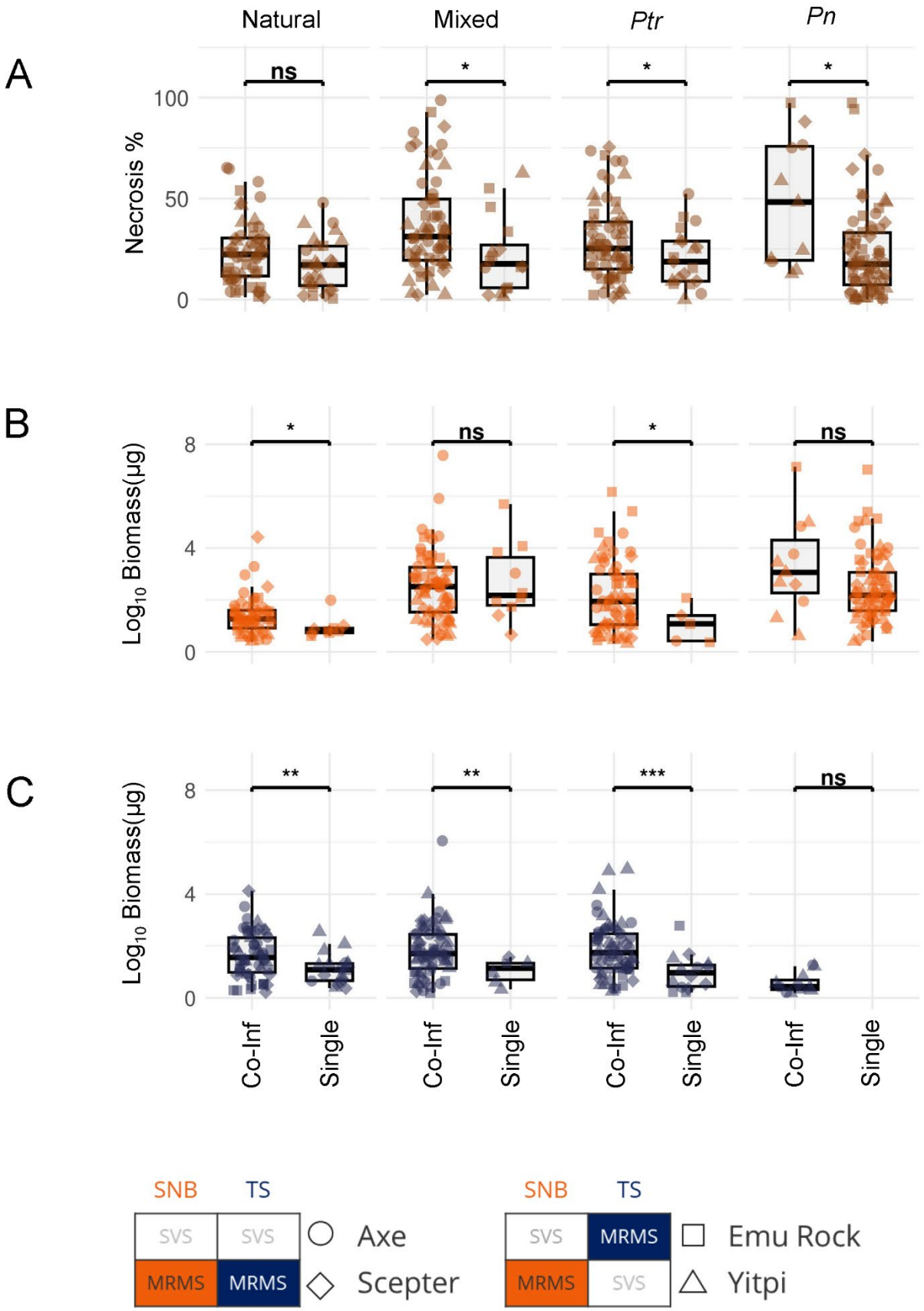
A
Natural
Mixed
Ptr
Pn
ns
*
*
*
Necrosis %
100
50
0
B
*
ns
*
ns
Log10 Biomass(µg)
8
4
0
C
**
**
***
ns
Log10 Biomass(µg)
8
4
0
Co-Inf
Single
Co-Inf
Single
Co-Inf
Single
Co-Inf
Single
SNB
TS
SVS
SVS
MRMS
MRMS
Axe
Scepter
SNB
TS
SVS
MRMS
MRMS
SVS
Emu Rock
Yitpi

Figure 5: Natural vs defined field inoculum

(A) necrosis severity (necrosis %, brown), **(B)** *P. nodorum* biomass (orange), and **(C)** *P. tritici-repentis* biomass (blue) across four field sites. Natural (naturally occurring infection in an endemic field Figure 4), Mixed (equal mix of *P. nodorum* and *P. tritici-repentis* infected stubble), *Pn (P. nodorum* infected stubble) and *Ptr* (*P. tritici-repentis* infected stubble). Points represent wheat leaf samples with shapes indicating wheat lines (circles = Axe, squares = Emu, diamonds = Scepter, triangles = Yitpi). Statistical significance of differences between co-infection and single infection within each site indicated above brackets (ns = not significant, * $p < 0.05$, ** $p < 0.01$, *** $p < 0.001$).

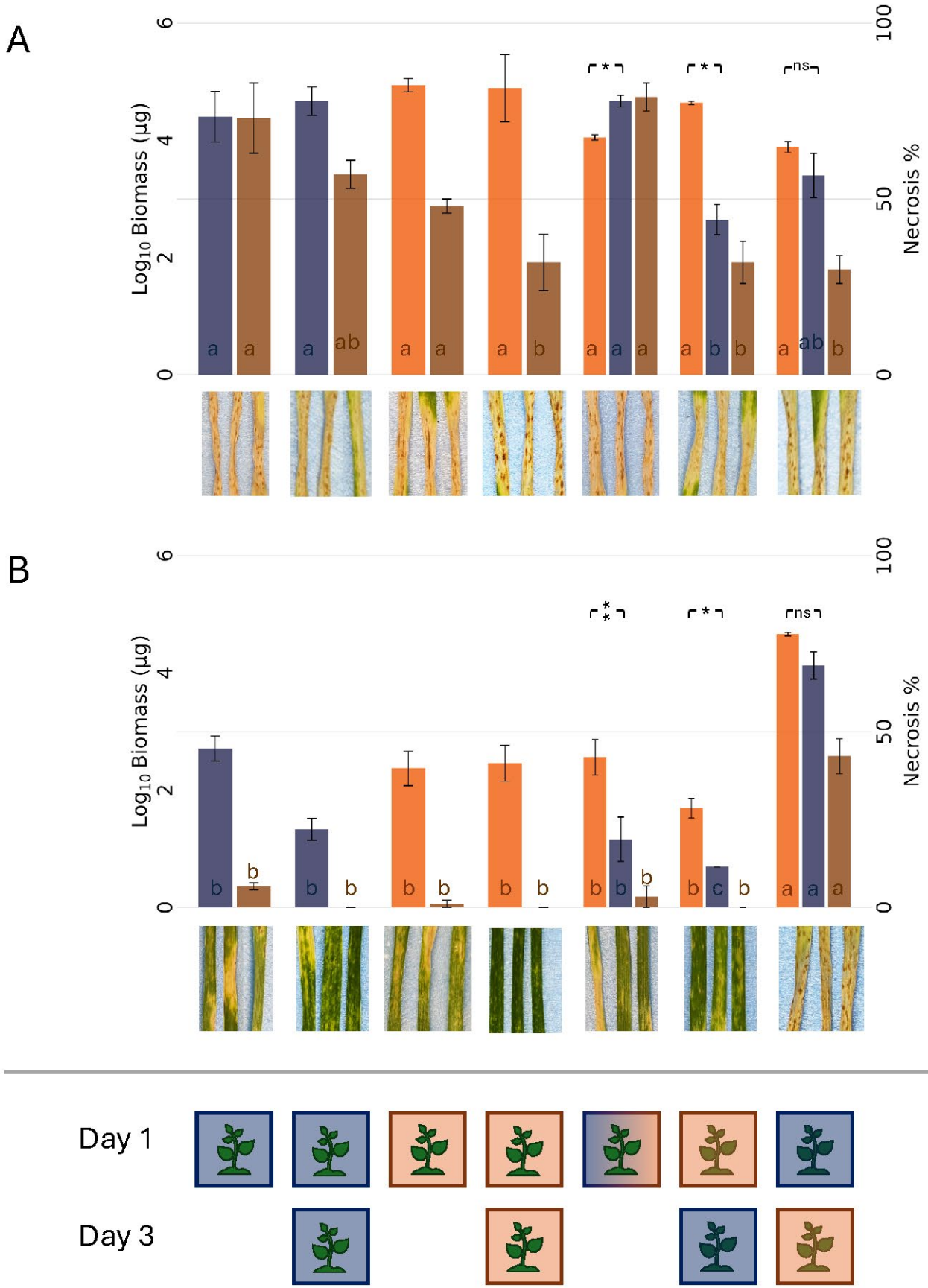
A
B
Log10 Biomass (µg)
Necrosis %
0
2
4
6
50
100
a
ab
b
c
*
**
ns
Day 1
Day 3

Figure 6: Sequential Seedling Infection

(A) Axe and **(B)** Scepter. Bars represent mean (±SE) $\log_{10}$ biomass (µg) for *Pn* (orange) and *Ptr* (blue), with Necrosis % (brown) plotted on the secondary y-axis. From left to right, Single pathogen treatments: Ptr → Ø Ptr → Ptr, Pn → Ø, Pn → Pn, Co-infection treatments: Pn + Ptr, Pn → Ptr, Ptr → Pn. Letters inside bars indicate statistical groupings within each series (Tukey HSD, $\alpha = 0.05$). Asterisks above bars indicate significant differences between *Pn* and *Ptr* biomass within co-infection treatments (paired t-test: ns = $p \geq 0.05$, * = $p < 0.05$, ** = $p < 0.01$,). n = 3 per treatment.